Compensated gadolinium-loaded plastic scintillators for thermal neutron detection and counting

Jonathan Dumazert, Romain Coulon, Guillaume H. V. Bertrand, Chrystèle Dehé-Pittance, Matthieu Hamel, Fabien Sguerra, Stéphane Normand, Laurence Méchin

Compensated gadolinium-loaded plastic scintillators for thermal neutron detection and counting

Jonathan Dumazert, Romain Coulon, Guillaume H. V. Bertrand, Matthieu Hamel, Fabien Sguerra, Chrystèle Dehé-Pittance, Stéphane Normand and Laurence Méchin.

***Abstract*–Plastic scintillator loading with gadolinium-rich organometallic complexes shows a high potential for the deployment of efficient and cost-effective neutron detectors. Due to the low-energy photon and electron signature of thermal neutron capture by gadolinium-155 and gadolinium-157, alternative treatment to Pulse Shape Discrimination has to be proposed in order to display a trustable count rate. This paper discloses the principle of a compensation method applied to a two-scintillator system: a detection scintillator interacts with photon radiation and is loaded with gadolinium organometallic compound to become a thermal neutron absorber, while a non-gadolinium loaded compensation scintillator solely interacts with the photon part of the incident radiation. Posterior to the nonlinear smoothing of the counting signals, a hypothesis test determines whether the resulting count rate after photon response compensation falls into statistical fluctuations or provides a robust image of neutron activity. A laboratory prototype is tested under both photon and neutron irradiations, allowing us to investigate the performance of the overall compensation system in terms of neutron detection, especially with regards to a commercial helium-3 counter. The study reveals satisfactory results in terms of sensitivity and orientates future investigation toward promising axes.**

I. Introduction

NEUTRON counting forms a critical branch of nuclear-related issues, whether flow monitoring on industrial infrastructures, dose rate monitoring for radioprotection or radiological material detection addressing CBRN threats [1] are concerned. More specifically, the last decade has been driven by the quest for competitive alternative technologies to neutron counters based on the helium-3 isotope, whose announced worldwide shortage has generated massive market value fluctuations [2]. In the meantime, the loading of plastic scintillators with gadolinium-rich organometallic complexes shows a high potential for the deployment of efficient and cost-effective detectors [3]. Gadolinium, indeed, through its naturally present 155 and (especially) 157 isotopes, exhibits the largest cross section (48890 barns) available among stable elements for the absorption of incident neutrons within the thermal energy range. A technical conundrum lies within the separation of the scintillation signal due to the prompt gamma rays most significantly emitted posterior to the (n,γ) neutron radiative capture from the scintillation signal attributable to ambient gamma-rays and falling into the same energy range. In default of any available Pulse-Shape Discrimination (PSD), the authors propose a neutron counting method on the basis of a robust compensation technique.

Jonathan Dumazert, Romain Coulon, Guillaume H. V. Bertrand, Matthieu Hamel, Fabien Sguerra, Chrystèle Dehé-Pittance and Stéphane Normand are with CEA, LIST, Laboratoire Capteurs et Architectures Electroniques, 91191 Gif-sur-Yvette, France (telephone: +33(0)169085324, e-mail: jonathan.dumazert@cea.fr).

Laurence Méchin is with CNRS (UMR6072), UCBN, ENSICAEN, Groupe de Recherche en Informatique, Image, Automatique et Instrumentation de Caen, 14050 Caen, France.

II. Related Work

Neutron detection represents a long-term technological challenge due to the indirectly ionizing nature of the radiation: the secondary particles generated after an interaction between a neutron and an atom of the sensor, which carry a charge, actually form the signature of the neutron presence. It is additionally imperative, when monitoring neutron activity, to discriminate this signature against the signal generated by secondary particles generated through the interaction between background photon radiation and the electrons of the sensor atoms.

Among the detectors specifically dedicated to thermal neutrons, helium-3 counters, which exploit a (n,p) type reaction with a thermal cross section equal to 5327 barns, are the most widespread [4]. Given the announced global shortage and strategic issues regarding tritium, alternative technologies to helium-3 are actively investigated, notably among plastic scintillators [5], which are low-cost (contrary to inorganic scintillators), easily scalable and shape-flexible, safer than their liquid counterparts due to their higher flash point. A straightforward exploitation of plastics quantifies the energy laid down by recoil protons [6] along the diffusion of incident rapid neutrons. To increase the responsivity to a neutron radiation, these plastics have to be loaded with thermal neutron adsorbing dopants, mainly [7-8] boron-10 or lithium-6. While these isotopes, as alpha particles emitters following neutron capture, easily allow a PSD between neutron and photon-generated pulses (the background photon signature being essentially formed of low-energy electrons and photons), their absorption thermal cross section, respectively equal to 3840 and 950 barns, is significantly lower than the one of their helium-3 competitor.

As already mentioned, natural gadolinium presents a 48890 barns cross section for the radiative (n,γ) capture of thermal neutrons [9] at 2200 $m.s^{-1}$. The loading of plastic scintillators with pure gadolinium or gadolinium-rich organometallic compounds aims at exploiting this exceptionally high cross section [10-11]. As most part of the exploited gamma response lies under 200 keV for small and medium-size scintillators, a major technical difficulty lies within the separation of the scintillation signal attributable to recoil electrons in the plastic matrix, generated after an interaction with electrons or photons present in the (n,γ) cascade, from recoil electrons due to an

interaction with background photons of comparable energy. Such drawback has motivated the authors of a reference patent application [12] to limit the scope of their invention, including gadolinium-loading, to configurations in which PSD remains possible. As an alternative to this approach, we hereby propose the transposition to gadolinium-based detection of a well-known measurement method in plastic scintillation [13-14], in which one makes use of two separate plastic scintillators with one them being, for instance, loaded with boron-10 or lihium-6 to be turned into a neutron-sensitive detector, while the unloaded second one remains solely sensitive to other types of radiations (photon, alpha).

III. Principle of a detection and counting method using photon response compensation

The principle of the neutron activity monitoring system disclosed is currently under patent deposition [15]. It is based on a two-scintillator compensation system:

- the first scintillator, named *detection scintillator*, interacts with photon radiation and is loaded with gadolinium element to become a thermal neutron absorber as well;
- the second scintillator, named *compensation scintillator*, is non-gadolinium loaded and therefore solely interacts with the photon part of the incident radiation.

The signature of the interaction between thermal neutrons and gadolinium may then be isolated by subtracting the compensation scintillator response to the total detection scintillator response, weighted by a coefficient representing their relative photon radiation responses.

A. Photon and electron signature of thermal neutron radiative capture by gadolinium-157 and gadolinium-155

Natural gadolinium (Gd) exists in the form of a combination of isotopes among which gadolinium-155 (14.7 % proportion, 61000 barns cross section) and mostly gadolinium-157 (15.68 %, 255000 barns) present an exceptionally high interaction probability with thermal neutrons [9].

The prompt source term associated with the de-excitation of a gadolinium following the absorption of a thermal neutron is subdivided into a prompt photon source term and a prompt electron source term. The complete equations of the nuclear reactions are presented in Eq. (1) and (2), where the sum of the gamma-rays labeled γ and the X-rays noted RX forms the photon source term, and the sum of internal conversion electrons noted CIe^- and the labeled Auger electrons Ae^- forms the electron source term.

$$^{155}_{64}\mathrm{Gd} + {}^{1}_{0}n \rightarrow {}^{156}_{64}\mathrm{Gd}^{*} \rightarrow {}^{156}_{64}\mathrm{Gd} + \gamma + RX + CIe^- + Ae^- \quad (1)$$

$$^{157}_{64}\mathrm{Gd} + {}^{1}_{0}n \rightarrow {}^{158}_{64}\mathrm{Gd}^{*} \rightarrow {}^{158}_{64}\mathrm{Gd} + \gamma + RX + CIe^- + Ae^- \quad (2)$$

As we primarily aim at the deployment of small and medium-volume scintillators (1 to 10 cm height and diameter), the exploitable signature is limited to the most significant electron terms and few hundred keV photon terms, which will significantly interact inside the sensors and thus induce a measurable scintillation signal. For the $^{157}_{64}\mathrm{Gd}(n,\gamma)$ radiative capture, the significant γ are emitted at 79.51 keV (0.773 per neutron capture abbreviated nc) and 181.931 keV (1.39 / nc) [16], together with the significant CIe^- associated with the first ray at 29.27 keV (0.348 / nc) [17] and accompanying X-rays [16] between 5 and 50 keV. For the $^{155}_{64}\mathrm{Gd}(n,\gamma)$ radiative capture, the significant γ are emitted at 88.967 keV (0.266 / nc) and 199.213 keV (0.389 / nc) [16], together with the significant CIe^- associated with the first ray at 38.73 keV (0.107 / nc) [17] and accompanying X-rays [16] between 5 and 50 keV.

Given the typical energy resolutions expected for the real plastic scintillator samples [18], typically of the order of 10 keV, we shall group these signatures into two energy windows $F_1 = [0; 100\ \mathrm{keV}]$ and $F_2 = [100\ \mathrm{keV}; 200\ \mathrm{keV}]$ over which selective countings should thus allow thermal neutron detection.

B. Detail of the system

The detection and compensation part of the device is represented by two equal-volume plastic scintillator, which may be concentric (for instance, two cylinders or spheres with the same geometry axis) or, as depicted on Fig. 1, non-concentric and with the same geometry. The detection scintillator (1) is loaded with gadolinium, under metallic or organometallic compound form, while the compensation scintillator (2) is non-gadolinium loaded. Both scintillators may optionally be isolated from photon background radiation by a lead or steel shield (3), in order to maximize the signal-to-noise ratio, completed by a thermalizing material for incident neutrons (for instance a certain thickness of polyethylene). Both scintillators are covered with reflectors (4) such as white paint to collect as many scintillation photons as possible, and an insulator layer (5) is inserted in between them so that a luminescence photon created in (1) may not be collected over the channel associated with (2) and vice versa. The conversions of the scintillation photons from (1) and (2) are respectively performed at the entrances of the amplified conversion systems (6) and (7). A high voltage supply (8) allows for the polarization of the conversion system so that the charges are multiplied. The compensation treatment of the electronic signals from (6) and (7) is achieved by dedicated electronics (9) connected to a computer (10). The block (9) composition is detailed in the next subsection.

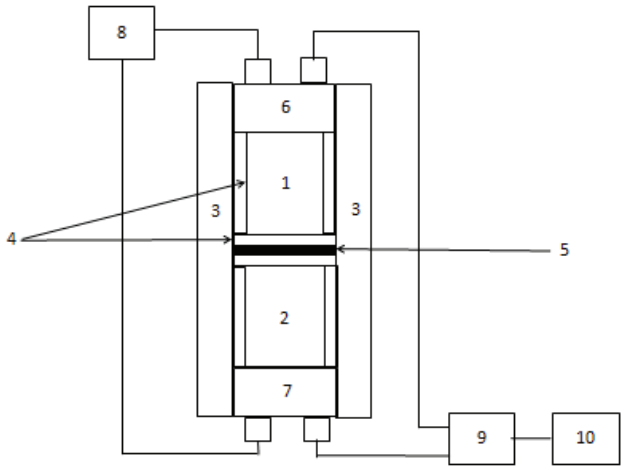

Fig. 1. Principle sketch of the detection system.

C. Detail of the electronics

The functional sketch of the electronics dedicated to the compensation operation is represented on Fig. 2. The voltages S_1 and S_2 from the conversion systems (6) and (7) of Fig. 1 are respectively collected on channels 1 (detection scintillator) and 2 (compensation scintillator). These signals may be pre-amplified in (1) to maximize the signal-to-noise ratio by charge integration. The signal pulses are then discriminated from noise in (2) by a level parameter, respectively V_1 and V_2, which may be an amplitude threshold, an area threshold, a duration threshold or any other triggering algorithm. Block (3) evaluates on each channel the deposited energy associated to the discriminated pulse P_1 or P_2: the maximum amplitude or the area is calculated and converted into energy E_1 or E_2 via an adequate conversion coefficient K_1 or K_2, known from previous calibration. A comparator with low and high energy thresholds tests whether E_1 or E_2 falls into one of the energy windows identified as relevant for neutron detection (the low boundary E_l may equal 0 or 100 keV and the high one E_h 100 or 200 keV). The detection may also be performed over the full energy spectra, in which case E_l and E_h are respectively set equal to 0 and infinity. Depending on whether E_1 or E_2 belongs to $[E_l\ ;\ E_h]$, an all-or-nothing signal TTL_1 or TTL_2 is delivered at the output of the comparator: 1 for one count, 0 for no count. With a temporal step Δt, a counter (5) is incremented from the outputs TTL_1 or TTL_2, and delivers a number of counts N_1 and N_2 over channels 1 and 2 respectively every Δt. The compensation between both channels is performed by modulus (6) and delivers a resulting count rate λ_n which is expected to provide an image of neutron activity. The concrete implementation of such compensation by the means of a hypothesis test will be thoroughly described in section V.

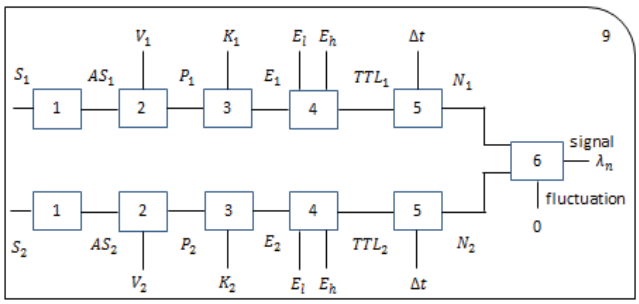

Fig. 2. Principle sketch of dedicated electronics.

IV. Estimation of the Photon Response Compensation Coefficient for Small-Volume Same-Geometry Gadolinium and Bismuth Loaded Plastic Scintillators

To validate the concept of the neutron detection and counting method exposed in section III, the neutron and photon radiation responses of small-volume same-geometry (as presented on Fig. 1) gadolinium-doped and non-gadolinium doped scintillating samples are assessed in terms of neutron counting over the full spectra and the relevant energy ranges F_1 and F_2.

A. Scintillating samples and acquisition setup

The gadolinium-loaded plastic scintillators are prepared as described by Bertrand et al. [19] and comprise:

- a reticulated polystyrene matrix;
- a reticulating agent;
- 2,5-diphenyloxazole (PPO) as a primary fluorophore;
- 1,4-Bis((2-methylstyryl)benzene) (Bis-MSB) as a secondary fluorophore;
- gadolinium tris-tetra-methylheptanedionate ($Gd(TMHD)_3$) as a gadolinium-rich organometallic compound.

The non-gadolinium loaded plastic scintillators for the photon response compensation may be prepared following the same recipe without the incorporation of $Gd(TMHD)_3$. However, the difference between the density and effective atomic number of gadolinium-loaded and non-gadolinium loaded samples is responsible for a dramatic dependence of the Q ratio of the counts registered in both scintillators with photon radiation energy for low energy radiation, mainly due to photoelectric effects [20], this dependence then disappearing for higher energy incident radiation. For the compensation to be easily implementable in variable energy distribution photon backgrounds, the coefficient Q should be as little dependent on the incident photon energy as possible over the widest energy range. Monte Carlo MCNPX simulations have shown that, for equal-volume scintillators, a significant decrease, reaching one order of magnitude, of the ratio between the maximum and the convergence value of Q may be achieved by introducing moderate bismuth loading of the non-gadolinium loaded scintillator performing the photon response compensation. This reduction is explained by the elevation of the effective atomic number of the resulting sample. The bismuth-loaded plastic scintillators are also prepared as described by Bertrand et al. and comprise:

- a reticulated polystyrene matrix;
- a reticulating agent;
- PPO as a primary fluorophore;
- Bis-MSB as a secondary fluorophore;
- triphenyl bismuth ($BiPh_3$) as a bismuth-rich organometallic compound.

As far as the quantitative compositions of the non-loaded, gadolinium-loaded and bismuth-loaded scintillator are concerned, the authors use the notations A, B and C and the compositions described in Table I.

TABLE I. Composition of Plastic Scintillators A, B and C

PS	$m_{monomers}$ (mg)	m_{PPO} (mg)	$m_{Bis\text{-}MSB}$ (mg)	m_{dopant} (mg)	wt% (metal)
A	2910	90	0.9	0	0
B	2625	85	0.9	290 ($Gd(TMHD)_3$)	2 (Gd)
C	2240	690	0.9	70 ($BiPh_3$)	1 (Bi)

The scintillating samples are then cut into a cylindrical shape and polished so that they meet the desired dimensions, i.e. 17.5 mm diameter and 8 mm height. Their lateral surface is ultimately covered with a reflecting white paint to limit the escape of scintillation photons.

Pulse height spectra are acquired using a Hamamatsu™ H1949-51 photomultiplier powered by an Ortec™ 556 High Voltage supply. Output signals are recorded unfiltered with a

custom made acquisition setup developed in our laboratory. The photomultiplier is isolated from ambient light and static noise sources inside an opaque Faraday cage.

B. Nonlinear energy calibration of the scintillators

In order to implement the photon response compensation of countings selectively registered over the energy windows F_1 and F_2, it is necessary, for each of the prepared samples A, B and C, to establish a correspondence between every channel in which counts are displayed and an energy value. As preliminary observations, notably reported by Bertrand et al., have shown that the calibration coefficient associating one energy value to one channel number, is not constant over F_1 and F_2 (a typical phenomenon at low energy, as for instance described by Williamson et al. [21]), but varies instead with the incident photon energy, we performed a nonlinear calibration of the three scintillators by making use of several gamma radiation sources available in the laboratory, positioned at a distance $d = 10$ cm of the scintillator surface along the symmetry axis of the scintillator:

- an americium-241 source whose photoelectric peak is observed at 59 keV ;
- a cobalt-57 source whose photoelectric peak is observed at 122 keV ;
- a cesium-137 source whose Compton edge is observed at 478 keV ;
- a sodium-22 source whose first Compton edge is observed at 341 keV and the second one at 1057 keV.

In the absence of any law assumption of the dependence of the conversion coefficient between an energy deposition and a given channel number, the experimental points are joined by line segments and the channel numbers respectively associated to both boundaries 100 keV and 200 keV are reported over one of these segments and enveloped in the uncertainty cylinder defined around the said segment based on the closer experimental values. The three calibration curves are superimposed on Fig. 3 with a semi-logarithmic scale.

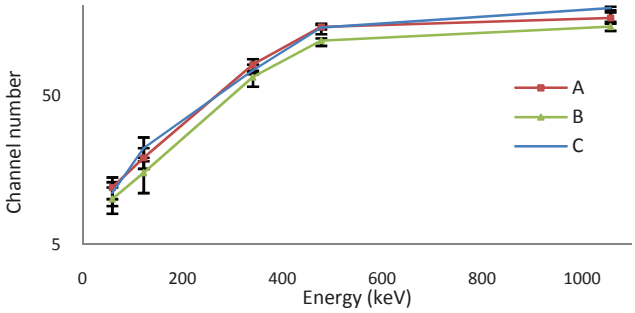

Fig. 3. Energy calibration curves of scintillators A, B and C.

C. Comparison between simulated and experimental compensation coefficients

Let N_A, N_B and N_C be respectively the counts registered with scintillators A, B and C in the presence of a given photon radiation source. These countings may be performed over the full energy spectra, i.e. all recording channels, or selectively over energy windows F_1 et F_2. We introduce the notations $Q_{B/A} = \frac{N_B}{N_A}$ and $Q_{B/C} = \frac{N_B}{N_C}$. These two ratios, which correspond the photon response compensation coefficients, are functions of the incident radiation energy E_γ. The first task is to compare the values for $Q_{B/A}$ and $Q_{B/C}$ experimentally obtained to the ones calculated by Monte Carlo calculations. The simulation describes as finely as possible the real samples by perfect cylinders of respective densities $\rho_{H1} = 1.1$ g.cm^{-3}, $\rho_{H3} = 1.2$ g.cm^{-3} and $\rho_{E2} = 1.1$ g.cm^{-3}. The MCNPX benz.01t material card is used to account for the styrene structure. $Q_{B/A}$ et $Q_{B/C}$ are calculated by simulation for a set of photon mono-energetic rays E_γ. We then experimentally compute these coefficient values from the energy spectra acquired in IV.B. with the three photon radiation sources we can approximate as mono-energetic: americium-241 (59 keV), cobalt-57 (122 keV) and cesium-137 (662 keV).

As illustrated on Fig. 4, Fig. 5 and Fig. 6 respectively for counts registered over the full energy spectra, F_1 and F_2, for B and C used in compensation, on Fig. 7, Fig. 8 and Fig. 9 respectively for counts registered over the full energy spectra, F_1 and F_2, for B and A used in compensation, the experimental values for the compensation coefficients match the simulation predictions as far as orders of magnitude and tendencies are concerned. They notably converge toward a value close to unity from incident energies superior to a few hundred keV. We furthermore note that, in accordance with simulation results, the difference between the experimental compensation coefficient at 59 keV and 662 keV is reduced when replacing the compensating scintillator A by C (as an example, for countings over F_1, $Q_{B/A}$ (59 keV) – $Q_{B/A}$ (662 keV) = 11.8 while $Q_{B/C}$ (59 keV) – $Q_{B/C}$ (662 keV) = 3.2).

Two major conclusions may be drawn from this confrontation between simulation and experiment results. Firstly, as a practical compensation requires the smallest possible dispersion of the compensation coefficient values, further work will solely be oriented toward an optimal loading of the compensating scintillator by heavy atoms such as bismuth. Secondly, the photon radiation background to which the gadolinium-loaded scintillator has to be compensated may be modeled by a linear combination of mono-energetic rays. As the detection test should calibrated to operate in the most versatile photon backgrounds, the conceiver needs as many degrees of freedom as possible for its study of the dependence of $Q_{B/C}$ with the incident energy distribution. The limited number of sources practically available in our laboratory and the conformity between simulation and experiment results thus lead to use simulation outputs for further calibration of the detection system.

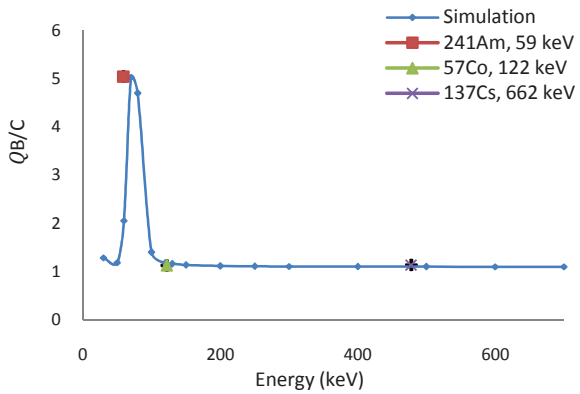

Fig. 4. Photon response compensation coefficient $Q_{B/C}$ as a function of energy for full spectra countings.

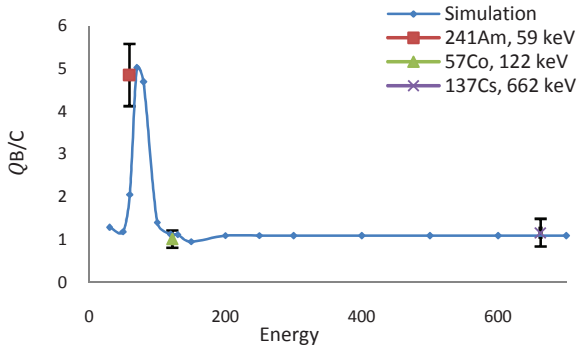

Fig. 5. Photon response compensation coefficient $Q_{B/C}$ as a function of energy for countings over F_1.

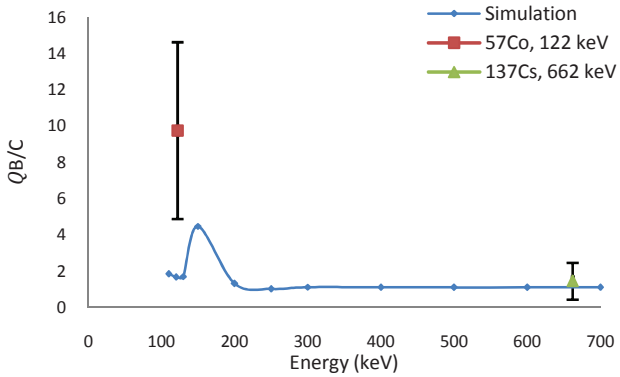

Fig. 6. Photon response compensation coefficient $Q_{B/C}$ as a function of energy for countings over F_2.

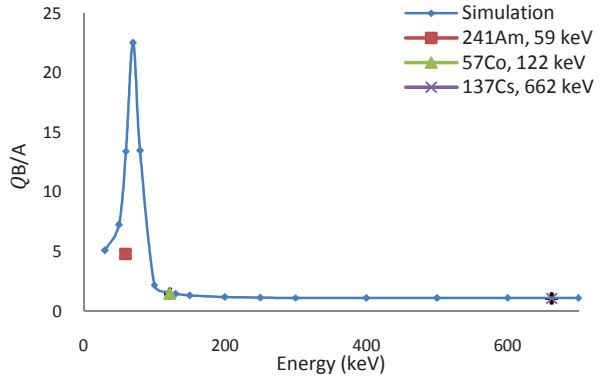

Fig. 7. Photon response compensation coefficient $Q_{B/A}$ as a function of energy for full spectra countings.

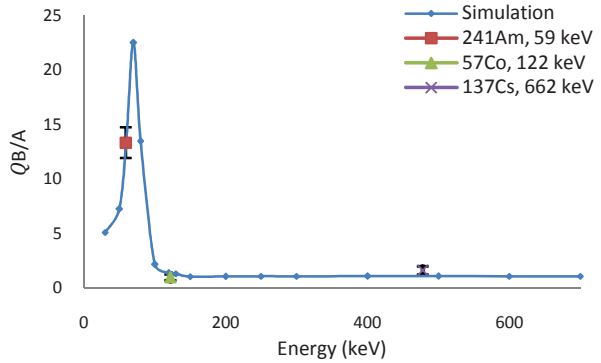

Fig. 8. Photon response compensation coefficient $Q_{B/A}$ as a function of energy for full spectra countings.

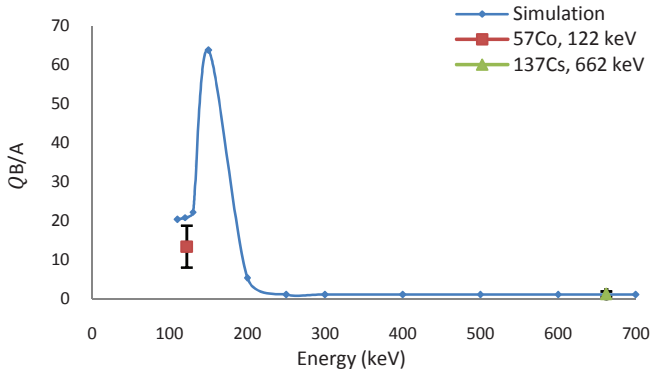

Fig. 9. Photon response compensation coefficient $Q_{B/A}$ as a function of energy for full spectra countings.

D. Estimation of the photon response compensation coefficient for neutron detection without a priori on the background energy distribution

In order to compute the values and associated standard deviations for the setting of the compensation coefficient when no *a priori* knowledge is available on the photon background energy distribution, this background is simulated with MCNPX code in the form of an isotropic emission spherical source at a distance $d = 10$ cm of the scintillator and whose energy is varied by discrete steps E_γ = {30 keV ; 50 keV ; 80 keV ; 100 keV ; 130 keV ; 150 keV ; 200 keV ; 300 keV ; 500 keV ; 1000 keV ; 1500 keV ; 2000 keV} for counting comparisons over the full spectra and F_1, and E_γ = {130 keV ; 150 keV ; 200 keV ; 300 keV ; 500 keV ; 1000 keV ; 1500 keV ; 2000 keV} over F_2. A preliminary run of simulations has enabled us to establish that for small-volume samples, anisotropy effects are negligible when compared with the compensation coefficient dependence on the incident photon energy, which justifies the choice of a spherical geometry for our simulation. In the absence of *a priori*, a uniform distribution law is postulated between the energy ray. If we label N_γ the number of simulated mono-energy ray, $E_{\gamma,i}$ for i varying between 1 and N_γ each of the energy ray, and $\Delta E_{\gamma,i} = E_{\gamma,i} - E_{\gamma,i-1}$ the uniform law ponderation coefficient associated with every energy ray (by construction, $\Delta E_{\gamma,1} = 0$), the expectation $\bar{Q}$ and the standard deviation $\sigma_{E_\gamma}(\bar{Q})$ associated with the compensation coefficient are estimated according to Eq. (3) and (4) respectively:

$$\bar{Q} = \frac{\sum_{i=2}^{N_\gamma} Q(E_{\gamma,i}) \cdot \Delta E_{\gamma,i}}{\sum_{i=2}^{N_\gamma} \Delta E_{\gamma,i}} \quad (3)$$

$$\sigma_{E_\gamma}(\bar{Q}) = \sqrt{\frac{\sum_{i=2}^{N_\gamma} \left(Q(E_{\gamma,i}) - \bar{Q}\right)^2 \cdot \Delta E_{\gamma,i}}{\sum_{i=2}^{N_\gamma} \Delta E_{\gamma,i}}} \quad (4)$$

The parameters for the photon response compensation obtained by treatment of the simulation results are presented in Table II for counting operations performed over the three considered energy ranges.

TABLE II. EXPECTED COMPENSATION COEFFICIENTS $Q_{B/C}$ AND ASSOCIATED DISPERSION STANDARD DEVIATIONS FOR COUNTINGS OVER THE FULL ENERGY SPECTRA AND THE ENERGY WINDOWS F_1 AND F_2

Parameter	Full spectrum	F_1	F_2
$\bar{Q}$	1.16	1.12	1.14
$\sigma_{E_\gamma}(\bar{Q})$	0.48	0.49	0.42

One may note that the expected compensation coefficients estimated over each of the three counting ranges are extremely close to the convergence values for this coefficient reached from 400 keV in the simulation results presented in *IV.C.*, respectively 1.10, 1.09 and 1.10 over the full spectra, F_1 and F_2. It follows that the asymptote of the compensation coefficient energy distribution, as well as its experimental value as a response to a cesium-137 source, provides a fair idea of the value for the useful parametrizing coefficient.

V. NONLINEAR SMOOTHING AND HYPOTHESIS TEST FOR NEUTRON DETECTION AND COUNTING

From the counts N_B and N_C, integrated over a 180 s temporal window (empirically identified as sufficient to achieve precise and stable count rate estimations), the average count rates on channel 1 (B) and channel 2 (C), respectively noted λ_B and λ_C, are computed by Eq. (5) and (6):

$$\lambda_B = \frac{N_B}{180} \tag{5}$$

$$\lambda_C = \frac{N_C}{180} \tag{6}$$

In order to simulate a realistic counting measurement, pulse frames $\boldsymbol{N_B^t}$ and $\boldsymbol{N_C^t}$ are created with a temporal step $\Delta t = 0.1$ s (compatible with real-time monitoring of the raw signals) on channels 1 and 2 by the means of the "Poissrnd" $\wp$ Matlab function, which generates random numbers N_B^t and N_C^t, composing the said vectors, following a Poisson-type probability distribution, respectively parametrized by λ_B and λ_C as made explicit on Eq. (7) and (8):

$$\forall\, t \in [0\,;180], N_B^t = \wp(\lambda_B \cdot \Delta t) \tag{7}$$

$$\forall\, t \in [0\,;180], N_C^t = \wp(\lambda_C \cdot \Delta t) \tag{8}$$

With such a small temporal step, the raw variance of the signals registered every Δt on channels 1 and 2 may tend to overcome the amplitude of the signal itself, especially at low count rates which are expected for small-volume sensors. This property of the counting signals prohibits the deployment of a sensitive hypothesis test quantifying a significant difference between both channels compared to the intrinsic level of statistic fluctuations expected on every one of them. It is beforehand necessary to apply a suited smoothing operation to the signals registered on channels 1 and 2.

A. Nonlinear smoothing of counting signals

In order to maintain a satisfactory level of count rate stability while allowing for a short response time variation monitoring of the radioactivity measured on channels 1 and 2, the authors have implemented on both channels a nonlinear smoother developed *ad hoc* in the laboratory for online nuclear counting measurements [22-23]. The principle of the smoothing operation is based on the adaptation of a retained window of count values for the estimation of the activity in accordance with the detection or non-detection of an abrupt change in the underlying Poisson statistics of the signal. The detection or non-detection is respectively determined by the acceptance or rejection of a centered Skellam statistics hypothesis, therefore justifying the Centered Skellam Test (*CST*) denomination for this smoothing method.

Previous works [24] have established the convergence of the method for count rates superior to 0.1 cps for an initial buffer size M exceeding 100 and described the optimization of the response time versus precision tradeoff as a function of the test parameter t_α. On the basis of these results, the authors have selected the values $M = 128$ and $t_\alpha = 1.4$ for the implementation of the *CST* smoother.

B. Hypothesis test for neutron detection

Let, after every fundamental time interval $\Delta t = 0.1$ s, $\widehat{N_B^t}$ and $\widehat{N_C^t}$ be the smoothed counting values exiting the *CST* smoother on channel 1 and 2 respectively. Let additionally $\sigma^2(\widehat{N_B^t})$ and $\sigma^2(\widehat{N_C^t})$ be the reduced variances respectively associated to $\widehat{N_B^t}$ and $\widehat{N_C^t}$ at the output of the smoother, $\bar{Q}$ and $\sigma^2_{E_\gamma}(\bar{Q})$ respectively the average compensation coefficient and its variance over a uniform energy distribution between 0 and 2 MeV. These notations are summarized on Eq. (9) and (10).

$$[\widehat{N_B^t}\,;\, \sigma^2(\widehat{N_B^t})] = CST(N_B^t) \tag{9}$$

$$[\widehat{N_C^t}\,;\, \sigma^2(\widehat{N_C^t})] = CST(N_C^t) \tag{10}$$

Every Δt, the following hypothesis test performs the detection and counting operation:

If:

$$\widehat{N_B^t} - \bar{Q} \cdot \widehat{N_C^t} > K \cdot \sqrt{\sigma^2(\widehat{N_B^t}) + \bar{Q}^2 \cdot \sigma^2(\widehat{N_C^t}) + \sigma_{E_\gamma}(\bar{Q})^2 \cdot \widehat{N_C^t}^2}$$

Then: $\widehat{N_n^t} = \widehat{N_B^t} - \bar{Q} \cdot \widehat{N_C^t}$

Else: $\widehat{N_n^t} = 0$

with K et $\widehat{N_n^t}$ being respectively the coverage factor parametering the test and the resulting counting signal, allegedly attributed to neutrons, deduced from the test. The values $\widehat{N_n^t}$ are stored in the temporal vector $\boldsymbol{\widehat{N_n^t}}$.

By dividing the resulting counts obtained every Δt by the temporal step, as made explicit in Eq. (11), an instantaneous count rate vector $\boldsymbol{\widehat{\lambda_n^t}}$ is obtained.

$$\boldsymbol{\widehat{\lambda_n^t}} = \frac{\boldsymbol{\widehat{N_n^t}}}{\Delta t} \tag{11}$$

C. Moving median for variance reduction of the resulting signal

A first image of the counting measurement is provided by the empirical temporal mean of the instantaneous count rate vector, labeled $\widehat{\lambda_n}$, around which an empirical variance $\sigma^2(\widehat{\lambda_n})$ is calculated to represent the dispersion of the actual instantaneous count rates around the mean. In practice, however, the frequency of the signal returns to zero also

provides a valuable piece of information to the operator about the significance of the detected activity. In order to account for this temporal behavior, as well as to reduce the resulting signal variance $\sigma^2(\widehat{\lambda_n})$, a moving median $\mathrm{med}(.,V)$ over a temporal window labeled V is applied to the count rate vector $\widehat{\boldsymbol{\lambda}_{\boldsymbol{n}}^{\boldsymbol{t}}}$, at the output of which a new rate vector is provided in Eq. (12).

$$\widehat{\boldsymbol{\lambda}_{\boldsymbol{n,V}}^{\boldsymbol{t}}} = \mathrm{med}\left(\widehat{\boldsymbol{\lambda}_{\boldsymbol{n}}^{\boldsymbol{t}}}, V\right) \tag{12}$$

An empirical mean $\widehat{\lambda_{n,V}}$ and an empirical variance $\sigma^2(\widehat{\lambda_{n,V}})$ are computed over this last vector. The size of the moving window has to be high enough to significantly lower the dispersion variance, and therefore improve the precision of the measurement, without inducing a prohibitively long response time or destroying the time-dependent information contained within the resulting signal. For the measurements presented in section VI, a satisfactory tradeoff has been empirically established for a window size $V = 300$ steps, i.e. 30 s. The temporal signal displayed after the moving median operation then represents a pseudo-real life measurement.

VI. Results

Four counting measurements are performed over 180 s with B (channel 1) and C (channel 2):

- measurement of the background radiation activity in the experiment room, labeled *background* measurement;
- measurement in presence of a *cesium-137* source of activity $A = 178$ kBq positioned at a distance $d = 10$ cm of the scintillator surface along the symmetry axis of the scintillator;
- measurement in presence of a *californium-252* source of activity $A = 1.2$ MBq with 10 cm High Density Polyethylene (HDPE) moderator in between;
- measurement in presence of an *americium-241* source of activity $A = 1$ kBq in contact with the scintillator.

The average count rates λ_B and λ_C obtained on each channel over the full spectra and energy windows F_1 and F_2 are listed in Table III.

TABLE III. AVERAGE COUNT RATES IN COUNT PER SECOND (CPS) WITH B AND C SCINTILLATORS OVER THE ENERGY RANGES OF INTEREST

Energy range \ Radioactive source	Background	Cesium-137 (10 cm)	Californium-252 (+ 10 cm HDPE)	Americium-241 (in contact)
Full spectrum	B : 2.3 C : 0.8	B : 308.5 C : 271.0	B : 83.6 C : 48.8	B : 8.5 C : 1.8
F_1	B : 2.0 C : 0.5	B : 127.9 C : 110.1	B : 48.7 C : 26.3	B : 7.1 C : 1.5
F_2	B : 0.1 C : 0.0	B : 59.5 C : 41.1	B : 10.1 C : 4.5	B : 0.4 C : 0.2

Fig. 10 to Fig. 12 present the average resulting count rates $\widehat{\lambda_{n,V=300}}$ provided by the simulator, together with their dispersion standard deviation $\pm\sigma(\widehat{\lambda_{n,V=300}})$, as a function of the test parameter K for measurements carried out on the full spectra and within the energy windows F_1 and F_2 respectively.

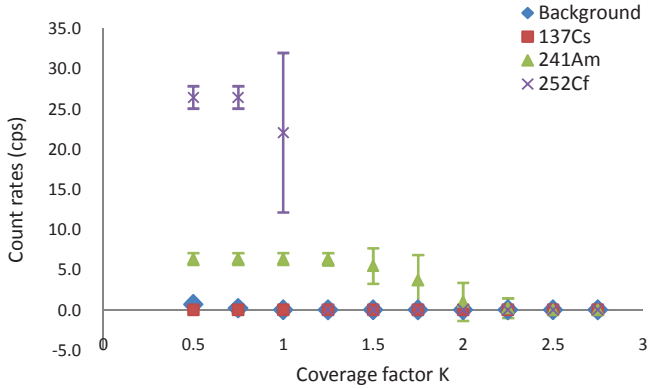

Fig. 10. Resulting count rate after the test (full spectra, $V = 300$) as a function of the coverage factor K.

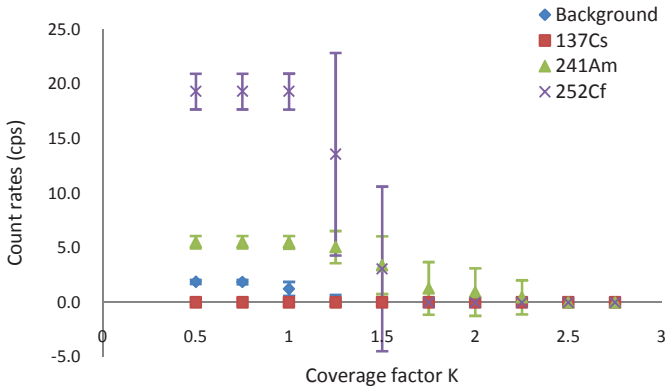

Fig. 11. Resulting count rate after the test (over F_1, $V = 300$) as a function of the coverage factor K.

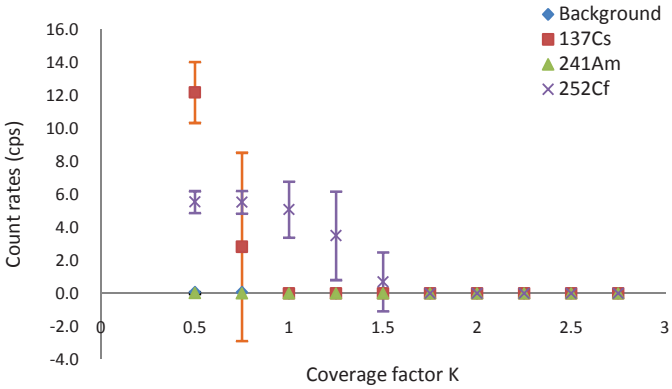

Fig. 12. Resulting count rate after the test (over F_2, $V = 300$) as a function of the coverage factor K.

VII. Discussion

Californium-252 is both a neutron and photon radiation emitter. The challenge of a photon response compensation for the californium-252 emission lies within the continuous nature of this emission between 0 and 10 MeV. It is however known that the prompt gamma emission is essentially at high energy [25], by 97 % superior to 140 keV and by 85 % superior to 300 keV, which mainly positions this emission within the convergence region for the photon response compensation coefficient and therefore leads us, in a first-order approach, to consider the compensation of a similar activity cesium-137 source as representative of the photon compensation for the californium-252 source. Furthermore, as C is not gadolinium-loaded, its response to the californium-252 source radiation

solely represents its response to the photon emission of the source, plus fast neutron diffusions which MCNPX simulations have shown to be negligible over such short acquisition time and interaction surface. One may note by reading Table 1 that 54 % of the counts induced in C by the californium-252 source lie within the energy range F_1 and 9 % in the range F_2, while, for the same sample, 41 % of the counts induced by the cesium-137 lie within F_1 and 15 % in the range F_2. Both photon response distribution are then indeed comparable, and the cesium-137 induced response in F_2, as far as the relative weight of the energy distribution is concerned, exceeds the one of the californium-252 source. Regarding the relative intensities of the responses, the data consigned in Table 1 reveal that the cesium-137 source induces in C six times as many counts as the californium-252 sources over the full spectrum, four times as many over F_1 and nine times as many over F_2. The compensation of the cesium-137 response thus clearly recovers the compensation for the photon emission of the californium-252 source as far as intensity is concerned over the three relevant energy ranges.

The value $K = 1$ for the test parameter ensures a null counting for the cesium-137 source as well as for the radioactive background over the three energy windows. As a result, the count rates associated with the californium-252 source for this value of K provide an indicative order of magnitude for the obtainable sensibility with the samples B and C used in compensation, $\widehat{\lambda_{n,V=300}} = 22.1 \pm 9.9$ cps, $\widehat{\lambda_{n,V=300}} = 19.3 \pm 1.6$ cps and $\widehat{\lambda_{n,V=300}} = 5.1 \pm 1.7$ cps respectively over the full spectra, F_1 and F_2. One may note that the utilization of the window F_1 allows for the reduction of almost one order of magnitude of $\sigma\left(\widehat{\lambda_{n,V=300}}\right)$ without any significant reduction of $\widehat{\lambda_{n,V=300}}$, as most of the counts lie within F_1. Nevertheless, because of the considerable distance between $Q(E_\gamma = 59 \text{ keV})$ from the americium-241 emission and the retained value for $\bar{Q}$, a significantly non null count rate is displayed in presence of the americium-241 source, until respectively $K = 1.75$ and $K = 1.5$ over the full spectra and F_1. This "false" neutron count rate, registered for a low activity source but positioned just on top of the sensor, underlines the impossibility of guaranteeing a robust neutron counting in a high intensity low energy (under 100 keV) photon radiation background for an integration over the full spectra and F_1 in the absence of any prior knowledge about the mean energy of the considered background. Reusing the notations from Eq. (3), to address this issue, one should first determine the energy distribution of the background activity $T\left(E_{\gamma,i}\right)$ and multiply this distribution with the entire $Q(E_{\gamma,i})$ spectrum to compute an actual value $\bar{\bar{Q}}$ which is suited for a representative compensation and calculated as presented in (13).

$$\bar{\bar{Q}} = \frac{\sum_{i=2}^{N_\gamma} Q\left(E_{\gamma,i}\right) \cdot T\left(E_{\gamma,i}\right) \cdot \Delta E_{\gamma,i}}{\sum_{i=2}^{N_\gamma} \Delta E_{\gamma,i}} \quad (13)$$

The obtained $\bar{\bar{Q}}$ coefficient, superior to $\bar{Q}$ in the case of a low-energy photon background, would then provide null count rate for the background measurement at the expense of a degraded neutron sensibility.

Another approach deduced from the displayed characteristics consists in solely working with the window F_2, which, by definition, is immune to photon radiation background under 100 keV. We consequently chose to compare the value for the resulting counting over this range for $K = 1$ as an image of the robustly identified neutron activity, i.e. $\widehat{\lambda_{n,V=300}} = 5.1 \pm 1.7$ cps, to a 65NH45 model helium-3 detector benchmarking measurement realized in the exact same condition with the same californium-252 source. The reference helium-3 count rate reaches 42.3 ± 5.9 cps for a 221 cm^3 active volume, to be compared with the 2 cm^3 volume of scintillating samples B and C.

VIII. Conclusion

The neutron measurement by compensation carried out over two small-volume same-geometry gadolinium and bismuth loaded plastic scintillators has allowed the detection of a neutron activity in the photon radiation background of the californium-252 source at the exit of the HDPE block (estimated about 1.7 Sv/h with a standard radiameter, which matches the typical constraints of a "monitored area" in the context of radioprotection applications). We have thus validated the concept of a new neutron detection system, portable and compatible with online implementation, whose first quantitative outputs promisingly compare to a commercial helium-3 detector. In order to increase the counting rates, as well as the precision associated to them, future works will be turned towards a scale-up over the loaded scintillating samples, with all the known challenges associated to such a process: homogeneity issues with the loading and self-absorption of the scintillator to quote the more obvious of them [26]. As far as the robustness of the detection is concerned, the main limitation arises from the distance between the values from the photon compensation coefficient under 200 keV and its mean and convergence values. Such distortion originates the notable distance between the interactions between low energy photon radiations and respectively the gadolinium and bismuth atoms. As a consequence, alternative elements to the bismuth will be investigated as dopants for compensation scintillator.

References

[1] "Chemical, biological, radiological or nuclear (CBRN) detection: a technological overview", NATO Parliamentary Assembly, pp. 18-20 (2005).

[2] "Managing critical isotopes, weaknesses in DOE's management of helium-3 delayed the federal response to a critical supply shortage", GAO-11-472, U.S. Government Accountability Office, Washington, D.C. (2011).

[3] Z. W. Bell, G. W. Brown, C. H. Ho, F. V. Sloop, "Organic Scintillators for Neutron Detection", X-ray and Gamma-ray Detectors and Applications IV, *Proc. of SPIE*, 4784, 150 (2002).

[4] D. A. Shea, "The helium-3 shortage: supply, demand and options for Congress", Congressional Research Service (2010).

[5] S. Normand, V. Kondrasovs, G. Corre, J.-M. Bourbotte and A. Ferragut, "MA-NRBC: First successful attempt for neutron gamma discrimination in plastic scintillators", *Proc. of ANIMMA* (2011).

[6] J R. Hansen, P. Reeder, A. Peurrung and D. Stromswold, "Neutron-gamma discrimination in plastic scintillators", *Nuclear Science Symposium, Conference Record. IEEE*, Vol. 2, pp. 1031-1035 (1998).

[7] R. J. Hu, J. H. Kim, S. H. Ahn, B. Hong, M. Ito, T. I. Kang, B. I. Kim, H. C. Kim, K. B. Lee, K. S. Lee, S. Park, M. S. Ryu and K. S. Sim, S. J. Hong, "Characteristics of boron-loaded plastic scintillators for neutron

measurements", *Journal of the Korean Physical Society*, **50**, *5*, pp. 1482-1488 (2007).
[8] R. D. Breukers, C. M. Bartle, A. Edgar, "Transparent lithium loaded plastic scintillators for thermal neutron detection", *Nuclear Instruments and Methods in Physics Research Section A*, Vol. 701, pp 58-61 (2013).
[9] D. A. Abdushukurov, *Gadolinium foils as converters of thermal neutrons in detectors of nuclear radiation*, Physics Research and Technology, p. 7 (2010).
[10] L. Ovechkina, K. Riley, S. Miller, Z. Bell, V. Nagarkar, "Gadolinium loaded plastic scintillators for high efficiency neutron detection", *Physics Procedia 2*, pp. 161-170 (2009).
[11] E. Velmozhnaya, A. Bedrik, P. Zhmurin, V. Titskaya, A. Adadurov, D. Sofronov, "Investigation of the behavior of gadolinium complexes in plastic scintillators", *Functional materials,* **20**, 4 (2013).
[12] N. P. Zaitseva, M. L. Carman, M. A. Faust, A. M. Glenn, H. P. Martinez, I. A. Pawelczak, S. A. Payne, K. E. Lewis, "System and plastic scintillator for discrimination of thermal neutron, fast neutron and gamma radiation" (2013).
[13] J. Bendahan, E. J. Morton, "Composite gamma-neutron detection system", US 8389941 B2 (2010).
[14] G. Daniel, E. Marienbach, J.–L. Szabo, Commissariat à l'Energie Atomique, "Process and apparatus for the simultaneous selective detection of neutrons and X or gamma photons", US 005481114 A, (1996).
[15] R. Coulon, J. Dumazert, G. Bertrand, M. Hamel, F. Sguerra, Commissariat à l'Energie Atomique et aux Energies Alternatives, "Dispositif de détection de neutrons et dispositif de comptage de neutrons thermiques associé" (2014).
[16] www-nds.iaea.org.htm
[17] bricc.anu.edu.au/index.php
[18] N. J. Cherepy, R. D. Sanner, T. M. Tillotson, S. A. Payne, P.R. Beck, S. Hunter, L. Ahle, P.A. Thelin, "Bismuth-loaded plastic scintillators for gamma spectroscopy and neutron active interrogation", *IEEE Nuclear Science Symposium and Medical Imaging Conference Record*, pp. 1972-1973 (2012).
[19] G. H. V. Bertrand, J. Dumazert, F. Sguerra, R. Coulon, G. Corre and M. Hamel, "Understanding behavior of different metals in loaded scintillators: discrepancy between gadolinium and bismuth", *Journal of Chemical Materials C*, accepted (2015).
[20] G. Knoll, *Radiation Detection and Measurement*, Fourth Edition, John Wiley & Sons, Inc., pp.47-49 (1999).
[21] J. F. Williamson, J. F. Dempsey, A. S. Kirov, J. I. Monroe, W. R. Binns and H. Hedtjärn, "Plastic scintillator response to low-energy photons", *Phys. Med. Biol.*, **44**, 857-871 (1999).
[22] V. Kondrasovs, R. Coulon and S. Normand, "Online method for measuring ionizing radiation", WO 2011101323 A1 (2011).
[23] V. Kondrasovs, R. Coulon and S. Normand, "An adaptative smoother for counting measurements", *Proc. of ANIMMA*, Vol. 1018 (2013).
[24] R. Coulon, V. Kondrasovs, J. Dumazert, E. Rohée and S. Normand, "Nuclear counting filter based on a Centered Skellam Test and a double exponential smoothing", *Proc. of ANIMMA*, submitted (2015).
[25] V. V. Verbinski, H. Weber, R. E. Sund, "Prompt Gamma Rays from ^{235}U(n,f), ^{239}Pu(n,f), and Spontaneous Fission of ^{252}Cf", *Physical Review C*, **7**, 3 (1973).
[26] J. B. Birks, *The theory and Practice of Scintillation Counting*, Pergamon Press, pp. 97-98, pp. 185-188 (1964).